Experimental Determination of the Diffusion Coefficients of Natural Oil/Wax Systems Using Microscope-Coupled Transmission Fourier-Transform Infrared Spectroscopy

A thesis presented to the faculty of the Graduate School of Western Carolina University in partial fulfillment of the requirements for the degree of Masters of Science in Chemistry.

By

Clarissa Mitchell

Advisor: Dr. Scott Huffman
Professor of Chemistry
Department of Chemistry & Physics

Committee Members: Dr. Carmen Huffman, Chemistry & Physics
Dr. Al Fischer, Chemistry & Physics

July 2024

ACKNOWLEDGMENTS

Thank you to: the Western Carolina Department of Chemistry and Physics, for providing me with the resources and funding to pursue a graduate degree, the WCU Chemistry Stockroom, for helping me secure materials I needed to complete this research, and the WCU Graduate School and the American Mosquito Control Association Research Fund for funding my research. A special thank you to my labmates, Taylor Gregory and Morgan Higgins, who helped in this method development project.

There are many individuals who were instrumental in my success during my undergraduate and graduate years. Not all are listed, but every instructor, colleague, or friend who has helped me understand something, listened to me talk, or just sat with me in the metaphorical trenches has my full gratitude and appreciation. Thank you to my advisor, Dr. Scott Huffman, and my committee, Dr. Carmen Huffman and Dr. Al Fischer, for the feedback and patience given during not only the duration of this research, but during my undergraduate years as well. I treasure the many hours I spent in Dr. Scott Huffman's office talking about research or life. Dr. Carmen Huffman's three semesters of teaching me how to be a chemist and not just study chemistry in seminar paid off tremendously, and I am eternally grateful for the multitude of professional and scientific skills that I learned under her tutelage. Thank you to Dr. DeSilva and Dr. Jamie Wallen for inspiring me to continue and for some of the best classes in which I had the opportunity to participate. Thank you to Dr. Alesia Jennings, for convincing me to pursue chemistry and for being a brilliant undergraduate advisor, I truly would not be here without her. A special thank you to my colleagues and friends Laura Hubler, Matteo Fratarcangeli, Hannah Bonogafsky, Reggie Hines, Savannah Mayer, and Kris Evans Newman, for their continuous encouragement and support. Finally, thank you to everyone outside of my academic life who has supported, encouraged, and kept me going through some of the most mentally challenging times of my life so far. Much love to you all.

TABLE OF CONTENTS

LIST OF TABLES

LIST OF FIGURES

LIST OF ABBREVIATIONS

D	Diffusion Coefficient
IR	Infrared
FT-IR	Fourier Transform Infrared
ATR-FTIR	Attenuated Total Reflectance Fourier Transform Infrared
micro-FTIR	Attenuated Total Reflectance Fourier Transform Infrared Microspectroscopy
PAN	Polyacrylonitrile
MCT	HgCdTe

ABSTRACT

EXPERIMENTAL DETERMINATION OF THE DIFFUSION COEFFICIENTS OF NATURAL OIL/WAX SYSTEMS USING MICROSCOPE-COUPLED TRANSMISSION FOURIER-TRANSFORM INFRARED SPECTROSCOPY

Clarissa Mitchell, M.S., Chemistry

Western Carolina University (July 2024)

Advisor: Dr. Scott Huffman

The goal for this research is to explore the process of select natural oils passively diffusing into a wax system to quantify the depth and speed of diffusion. Studying the diffusion process in these systems can provide valuable insight into the physical interactions between the wax and diffusant molecules and into the mechanics of diffusion-based solvation. The waxes used in this system are beeswax, paraffin wax, and carnauba wax, used with d-limonene, α-pinene, β-pinene, l-carvone, and cinnamaldehyde as the diffusants. The diffusion coefficient for each system was determined by the timed acquisition of infrared spectra using transmission Fourier-transform infrared spectroscopy and generating diffusion profiles per oil/wax system by plotting the changing absorbance of the diffusant band verses time. Selected points were chosen and fit linearly to solve for the diffusion coefficients. The average diffusion coefficients were determined to be: 93.4$\pm$32.6 μm^2/s for d-limonene/paraffin wax; 74.9$\pm$17.5 μm^2/s for d-limonene/beeswax; 76.379$\pm$0.005 μm^2/s for α-pinene/paraffin wax; 86.9$\pm$47.4 μm^2/s for α-pinene/beeswax; 45.571$\pm$0.005 μm^2/s for β-pinene/paraffin wax; and 96.4$\pm$22.0 μm^2/s for β-pinene/beeswax. No diffusion was measured for l-carvone, cinnamaldehyde, or carnauba wax systems. It was found that d-limonene, α-pinene, β-pinene, and l-carvone could dissolve beeswax and paraffin wax. Cinnamaldehyde could not dissolve any wax. Carnauba wax was not dissolved by any diffusant.

CHAPTER ONE: INTRODUCTION

Background

Motivation

Mosquitoes are considered one of the deadliest disease vectors in the world. According to the 2022 World Malaria Report from the World Health Organization (WHO), there were approximately 725,000 deaths globally from mosquito-borne illnesses, 600,000 of those being from malaria.[1] One option to mitigate the health crisis of mosquito-borne diseases is to reduce the number of active vectors by killing adult mosquitoes with insecticides. In addition to being costly and time-intensive, these vector control methods will often use only one or two types of insecticides for a large area. As a result, mosquitoes are starting to become resistant to the insecticides.[2] The WHO reported that 78 countries worldwide reported insecticide resistance to at least one of the four classes of insecticides, and 29 countries reported resistance to all four main classes.[1] This resistance to the effectiveness of vector control could potentially increase death and transmission rates of mosquito-borne illness worldwide. One way to combat insecticide resistance is to circumvent the mutations mosquitoes have developed that inhibit insecticide from reaching their biological target. Since the common classes of insecticides are thought to rely on diffusion through the mosquito exoskeleton, improved understanding of diffusion characteristics could drive the development of more effective pesticides. Developing a method to study the nature of liquid diffusion through a solid substrate could be valuable.

Vector Control

There are four main classes of insecticides used in vector control: pyrethroids, organophosphates, carbamates, and organochlorines.[3] These insecticides are used across the world to reduce the number of viable vectors. The two avenues of vector control are targeting the larval mosquitoes or the adult mosquitoes. According to the Center for Disease Control, local governments and mosquito control districts control adult populations of mosquitoes by spraying adulticides, organophos-

phates, plant-derived pyrethrins, and synthetic pyrethroids, into the air and onto the surfaces on where the mosquitoes may land.[4]

The most used types of insecticide, pyrethrins and pyrethroids, kill mosquitoes by interfering with the nervous system of the mosquito, which resides underneath the exoskeleton of the mosquito.[3] The arthropod exoskeleton consists of layers of cuticle, composed of chitin, protein, and lipids, with a layer of cement and wax on the outermost layer of the insect.[5] This outer layer waterproofs the mosquito. When a mosquito lands on a sprayed surface or makes contact with an insecticide in the air, the molecules must diffuse through the waxy outer layer and cuticle layers to reach the nervous system. Mutated resistance may be inhibiting the uptake of insecticide by preventing the diffusion of the insecticide to the mosquito nervous system.[6]

Mutated Resistance

One of many proposed mechanisms of insecticide resistance is a mutated cuticle to reduce the penetration of the insecticide into the mosquito nervous system.[2,7] One such mutation could be a thickening of the cuticle. One study found a 10% thicker cuticle on the legs of pyrethroid-resistant or tolerant mosquitoes compared to the cuticle of the non-resistant mosquitoes.[8] Another study found that the penetration of deltamethrin, a pyrethroid, was significantly slower in resistant cotton bollworms.[9] These results could mean that the molecules of the insecticide have difficulty crossing the potentially thickened cuticle of the resistant mosquito. In addition to the mutation of the physical attributes of the cuticle, the chemical composition of the cuticle could also be altered by mutation to prevent the uptake of the insecticide.[10]

Norris and Bloomquist (2021) have shown that by mixing select natural oils in with pyrethrins, the toxicity of the insecticide was increased in resistant mosquitoes.[6] One proposed mechanism for this increase in toxicity is that the penetration of the insecticide is increased by “improved passive diffusion”, or that the additives in the insecticides are cooperatively supporting movement of the insecticide through the cuticle. Measuring the rate of diffusion could be useful to continue to study how additives in insecticides can enhance the penetration and thus the effectiveness of

the active ingredients in the insecticide.

Diffusion

Diffusion is a physical process that is widespread through the natural and synthetic world and governs countless biological systems, pharmacological processes, and industrial avenues. Diffusion can be described as the rate of change in concentration of diffusant with respect to time. This approach to diffusion physics is mathematically represented by Fick's second equation

$$\frac{\partial C}{\partial t} = D\frac{\partial^2 C}{\partial x^2} \tag{1}$$

where C is the concentration of the diffusant, t is time, x is the spatial parameter of the diffusion and D is a proportionality constant that is known as the diffusion coefficient, or diffusivity, (D) with the SI units $\frac{m^2}{s}$. The diffusion results of this research are given in μm^2/s. D describes how quickly a certain diffusant will move through a certain medium; a larger D indicates faster diffusion. Diffusivity can be affected by atmospheric pressure and temperature. Determining the diffusivity of a system can help to understand the chemical and physical interactions of the components of the system, allowing research into the nature of diffusion itself.

Infrared Spectroscopy

Fourier-transform infrared spectroscopy (FT-IR) is a form of vibrational spectroscopy that uses infrared (IR) wavelengths of light to analyze chemical compounds. Covalent bonds absorb infrared light at wavelengths specific to the energy of the bond and the technique yields a highly informative absorbance spectrum that displays absorbance bands by wavenumber (cm^{-1}). Quantitative chemical analysis of mixtures using IR spectroscopy relies on the Beer-Lambert law

$$A = \varepsilon\, b\, C \tag{2}$$

where A is absorbance, ε is molar absorptivity, b is path length, and C is concentration. Two main techniques of FT-IR are used widely based on how the light is detected: reflectance and

transmission. Reflectance measurements are collected using attenuated total reflectance (ATR) where the IR light measured is reflected off the sample. Transmission measurements are acquired by detecting the transmitted light through the sample. This technique generally relies on a sample holder for measurements and requires the light to be able to pass through the sample. Transmission FT-IR is used for this experiment.

Infrared microspectroscopy (micro-FTIR) measures the absorbance spectrum of a small area of a sample using transmitted IR light. This technique is contrasted with the typical ATR-FTIR techniques which measure the chemical sample in contact with the ATR crystal. Micro-FTIR is useful for spatial measurements and allows data collection of a specific section of the sample. Visual microscopy can be used in conjunction with this technique to obtain both an absorbance spectrum and a visual image of a small section of the sample. Imaging and collection of infrared spectra of a specific area in a sample makes micro-FTIR a suitable choice for the method development of this diffusion project.

Measuring Diffusion using Infrared Spectroscopy

Typically, the D of liquid-liquid systems can be be determined by dynamic light scattering analysis (DLS), but this method does not translate to a solid-liquid system such as the penetration of insecticide into a cuticle. Using micro-FTIR to measure D relies on the Beer-Lambert law (Equation 2). Assuming that the Beer-Lambert law holds true, the concentration of diffusant would be proportional to the intensity of the absorbance bands of diffusant in the infrared spectrum of the analyzed system. Using absorbance as a proxy measurement for concentration requires that the other parameters of the Beer-Lambert law (ε, and b) remain constant.

The general method for measuring diffusion with infrared spectroscopy involves acquiring a number of infrared spectra over a set period of time and observing how the absorbance changes as the concentration of diffusant changes. This experiment is established using attenuated total reflectance Fourier transform infrared (ATR-FTIR) spectroscopy.[11–18] In ATR-FTIR diffusion experiments, the material that will be diffused into sits on top of the ATR crystal and the diffusant

is then applied to the top of the material. The infrared spectra taken at different times will change as the diffusant diffuses through the material until reaching a plateau of diffusive equilibrium. McAuley et al., (2010) used ATR-FTIR to study the effects of select solvents on the diffusion of a model compound (4-cyanophenol, or CNP) across a silicone membrane.[12] The researchers were able to determine D for CNP and several solvents into the silicone membrane, and characterized the effects of the solvents on the diffusion rate of CNP into the membrane. This characterization of diffusion by system resembles closely the type of experiment that this research seeks to perform.

The use of transmission infrared spectroscopy to conduct diffusion-related experiments is less documented. A study from 1992 by High et al. detailed using transmission infrared spectroscopy to measure the mutual diffusion of two polymer films into each other.[19] Researchers used two KBr windows coated with the polymer films separately and the beam of infrared light passed through the cell to collect spectra every 3-4 hours. As the spectrum changed, the researchers were able to utilize the changing absorbance to calculate a D of the two polymers diffusing into each other.

Diffusants

This research uses five diffusants, the structures and characteristics of which are shown in Table 1. The diffusants used were readily accessible and were chosen for the presence of resolved vibrational bands located in the functional group region of the IR spectrum. Almost all of the diffusants are terpenes, a class of naturally synthesized molecules with the base formula $(C_5H_8)_n$ where n $\geq$ 2.[20] Terpenes are an important class of molecules that are widespread and diverse in structure. A monoterpene has the basic formula $C_{10}H_{16}$ and can be acyclic or cyclic.

Three diffusants used are monoterpenes: d-limonene, α-pinene, and β-pinene . All three of these molecules are cyclic and have the same molecular weight, 136.23 g/mol. d-limonene, marked by a sweet, citrus smell, is the most common isomer of limonene and is mostly obtained from citrus peels. d-limonene is used widely industrially as a flavoring agent, a solvent for oils

Table 1. Diffusant characteristics.

Diffusant	d-limonene	α-pinene	β-pinene	l-carvone	Cinnamaldehyde
Mass (g/mol)	136.23	136.23	136.23	150.22	132.16
Classification	Monoterpene	Monoterpene	Monoterpene	Terpenoid	Phenylpropanoid
Relative Polarity	Nonpolar	Nonpolar	Nonpolar	Semi-polar	Most polar
Relative Flexibility	Most flexible	Slightly flexible	Slightly flexible	Semi-flexible	Least flexible
	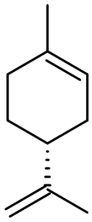	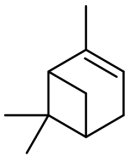	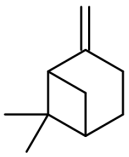	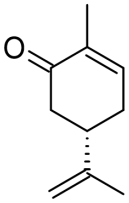	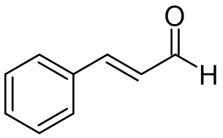

and glues, and as a scent in a variety of perfumes and soaps.[21] α-pinene and β-pinene are bicyclic and geometric isomers of each other. Pinenes are isolated from turpentine, a natural product obtained from pine trees, among other natural sources. α-pinene is the most prevalent compound in turpentine and is used more broadly than β-pinene, but both pinenes are widely used in the industrial and consumer sector.

Another diffusant is a modified terpene, known as a terpenoid: l-carvone ($C_{10}H_{14}O$, 150.22 g/mol), which has a ketone attached to the ring of the terpenoid. l-carvone has a minty and savory smell and is found in concentration in and spearmint.[22] l-carvone was certified in 2009 by the United States Environmental Protection Agency (EPA) as an effective mosquito repellant.[23] Both l-carvone and d-carvone are used widely in flavoring, agriculture, and organic synthesis.[24]

The last diffusant used is cinnamaldehyde (C_9H_8O) which is not of the terpene classification, but is also a naturally derived molecule belonging to the phenylpropanoid family.[25] Cinnamaldehyde is found in nature primarily in its trans isomer and has a molecular weight of 132.16 g/mol. It is responsible for the taste of cinnamon and is used in flavorings widely. Cinnamaldehyde is also an effective insect repellent and mosquito larvicide.[26,27]

These five molecules can be sorted by polarity and by bond flexibility which can be found in

Table 1. The least flexible molecule is cinnamaldehyde, due to the conjugation of the bonds and rigid ring structure. Cinnamaldehyde is also the only planar diffusant and has a polar aldehyde group on one end of the molecule. The isomers α-pinene and β-pinene are also rigid molecules exhibiting a bridged ring resulting in a bicyclic, bulky structure. β-pinene is slightly more flexible than α-pinene because the double bond is at position 1 at the edge of the molecule instead of in the ring like in α-pinene. l-Carvone is identical in structure to limonene save for the added ketone in position 2 on the unconjugated ring and would be more flexible than the pinenes and cinnamaldehyde due to the number of single bonds and branching methyl groups. The ketone also adds an element of polarity. Limonene lacks any polar functional groups and is the most flexible of the diffusants.

Waxes

Waxes are chemically heterogeneous solids with varying chemical composition. They are solid at room temperature and hydrophobic. Waxes can be naturally synthesized through plants or animals or synthetically derived. The substrate for these experiments were three different waxes: carnauba wax, paraffin wax, and beeswax. These waxes and their characteristics are shown in Table 2. The wax is used as a model system to emulate the waxy cement layer on the exoskeleton of arthropods. These waxes were chosen because they were readily available and because they are commonly researched and used waxes.

Table 2. Wax characteristics.

Wax	**Density (g/cm^3)**	**Melting Point (°C)**	**Relative Polarity**
Carnauba	0.990-0.999	83.0-84.0	Most polar
Beeswax	0.921-0.957	64.6-65.1	Semi-polar
Paraffin	$\sim$0.900	57.4-58.2	Least polar

Carnauba wax comes from the Brazilian carnauba palm and is used widely in many goods produced, including polishes for leathers and hard candies, cosmetics, and can be used to alter consistencies of solvents and printing inks. Carnauba wax also has a relatively higher melting point range from 83.0-84°C and is a brittle wax that is usually mixed with beeswax to yield a more pliant wax.[28] The density of carnauba wax ranges from 0.990 to 0.999 g/cm^3.[29] Chemically, the wax is primarily composed of aliphatic esters and alcohols (52%), with little saturated hydrocarbon content (1%).[29] Processed carnauba wax is usually found as yellow, shiny, brittle flakes.

Paraffin wax is a petroleum-derived wax which has uses in lubrication, coatings, candles, and crayons. The composition of paraffin wax includes primarily long-chained saturated hydrocarbons, ranging from 20-30 carbons in length.[30] Paraffin wax is a white, slippery wax with a melting point range from 57.4-58.2°C. The density of paraffin wax ranges with purity but is around 0.900 g/cm^3.[31]

Beeswax is produced by bees to create the structures of their hives. Beeswax has many applications and one of the oldest waxes to be used by humanity. Modern uses of beeswax include in pharmaceuticals, coatings, cosmetics, candles, food processing, and industrial products.[32] The beeswax used in this research was harvested in Cullowhee, North Carolina by a local bee farmer. The wax was purified by melting and filtering the insect debris out of the liquid. Beeswax is bright yellow and rubbery with a density of 0.921-0.957 g/cm^3 and a melting point range of 64.6-65.1°C.[33] Beeswax composition has more saturated hydrocarbon content than carnauba wax (67%), but less than paraffin waxes.[34] It is also composed of fatty acids, monoesters, and diesters.[35]

All waxes, by nature, are hydrophobic and are considered nonpolar. By analyzing relative saturated hydrocarbon content and the presence of esters or alcohols attached to the hydrocarbons in the matrix of the waxes, the waxes can be sorted by relative polarity. The carnauba wax has the smallest saturated hydrocarbon content and will be considered as the most polar wax while the paraffin wax, almost completely composed of saturated hydrocarbons, will be considered the

least polar wax. Beeswax has a middle-ground relative polarity and is used as an in-between carnauba wax and paraffin wax in terms of polarity. Carnauba wax is the most dense wax, followed by beeswax, and paraffin wax is the least dense.

Data Analysis

Diffusant Analytical Wavelength

The diffusant analytical wavelengths used for data processing are tabulated in Table 3. This research uses transmission IR spectroscopy and needs a platform for the oil/wax system to rest on while the measurements take place. This research uses glass microscope slides that have been cut into smaller pieces to hold the wax. The diffusant is later introduced on the bottom glass slide and the absorbance spectrum is measured over time. Glass absorbs IR light from 650-2200 cm^{-1} which encapsulates the fingerprint region where the majority of the diffusant IR absorbance occurs. There is a broad band for each diffusant and wax in the functional region located from 2700-3150 cm^{-1} which corresponds to the C-H stretching mode. Limonene, β-pinene, and carvone have a small variation in this band that is different from the wax spectra at 3075 cm^{-1}, which is used as the analytical wavelength for these diffusants. α-pinene has a band centered at 3025 cm^{-1}. These bands were chosen because they are resolved from the broad C-H stretching band. Cinnamaldehyde has a small band centered at 3335 cm^{-1}, which serves as the analytical wavelength.

Table 3. Diffusant analytical wavelengths.

Diffusant	**Wavenumber (cm^{-1})**
d-limonene	3075
α-pinene	3025
β-pinene	3075
l-carvone	3075
Cinnamaldehyde	3335

Determining Diffusion Coefficient

The mathematics for determining the diffusivity of a system were used from a study from Fieldson and Barbari, (1993), where they were measuring the D of water and polyacrylonitrile (PAN).[13] The researchers used Fick's second equation, (1), and used a method of sorption kinetics where the sorbed mass changes as a function of time. By applying the boundary conditions of a short time of measurement and assuming the pool of water was infinite, the authors derived the following equation,

$$\frac{M_t}{M_\infty} = \frac{2}{L}\left(\sqrt{\frac{t}{\pi}}\right)\sqrt{D} \tag{3}$$

where $\frac{M_t}{M_\infty}$ is equal to the mass sorbed by the PAN and L is the thickness of the PAN. This equation describes the initial diffusion of water across the PAN, which is linear in nature. Fieldson and Barbari used ATR-FTIR for this project and L describes the distance downward the water travels to reach the ATR crystal. This equation can be applied to this research to calculate the D of natural oils and different waxes. This research uses IR spectroscopy to determine the absorbance of a diffusant at a certain position in a thin layer of wax. Unlike Fieldson and Barbari, this research uses transmission IR spectroscopy so the orientation of the experiment changes and the diffusant travels laterally through the wax instead of vertically. Assuming that the Beer-Lambert law, 2, holds true, the absorbance of the diffusant can be used as a proxy measurement for the concentration of the diffusant. $\frac{M_t}{M_\infty}$ from Equation 3 is a concentration parameter and can be renamed as the absorbance of diffusant, $\frac{A}{A_{max}}$, and L can become Δx to represent the lateral distance into the wax the beam path of the transmitted IR light, as shown in Figure 3. These substitutions yield:

$$\frac{A}{A_{max}} = \frac{2}{\Delta x}\left(\sqrt{\frac{t}{\pi}}\right)\sqrt{D} \tag{4}$$

Plotting absorbance values at the analytical wavelength versus time creates a sigmoidal diffusion

profile. Using the most linear section of the diffusion profile, the linear points can be normalized to the absorbance max and plotted versus $\sqrt{t}$. The slope of this linear fit is

$$\text{slope} = \left(\frac{2}{\Delta x} \sqrt{\frac{D}{\pi}} \right) \tag{5}$$

By solving Equation 5 for D, the diffusion coefficient can be calculated using the determined slope.

$$D = \pi \left(\frac{(\text{slope})\Delta x}{2} \right)^2 \tag{6}$$

Hypothesis

This research seeks to explore the physical-chemical nature of the diffusivity of the diffusants and waxes described above. These systems are meant to model the diffusion of compounds through the cuticle of a mosquito exoskeleton. By using micro-FTIR to determine D for each system, some information regarding the interactions of the diffusant molecules through the matrix of the wax can be discovered. Each diffusant and wax couple combines different attributes like shape of the diffusant, polarity of the diffusant and waxes, and density of the wax. Comparing the D of each system can provide insight into the interactions of the diffusants and wax. Table 4 contains the characteristics of each system and a predictive ranking of which systems are hypothesized to have the fastest rate of diffusion. The intermolecular interactions between the diffusants and waxes are likely the strongest contributor to the rate of diffusion. Weak intermolecular forces, such as London forces between two nonpolar molecules, are faster than stronger, polar interactions, so nonpolar systems would be characterized by larger diffusion coefficients. Flexibility of the molecule could also play a significant part in determining the rate of diffusion; a more flexible molecule could diffuse faster through a more dense wax as it interacts with the wax molecules more completely.

The hypothesis for this research is that the diffusivity of a system can be correlated to the

structure and characteristics of the molecules involved; that is, a more nonpolar diffusant will move through a more nonpolar wax more quickly, or a more rigid diffusant will not diffuse as quickly through a dense wax, and vice-versa. Ultimately, the interactions between the molecules could directly affect the diffusivity of a system and studying them can help to understand exactly what makes certain molecules diffuse through solids faster or slower, which could be valuable for insecticide diffusion research. This project also describes a new method for determining the diffusion coefficient of solid/liquid systems.

Table 4. Predicted diffusion coefficients per system and material characteristics.

			Diffusant	d-limonene	α-pinene	β-pinene	l-carvone	Cinnamaldehyde
			Relative polarity	Nonpolar	Nonpolar	Nonpolar	Semi-polar	Most polar
			Relative flexibility	Most flexible	Slightly flexible	Slightly flexible	Semi-flexible	Least flexible
			Structure	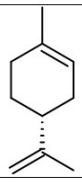	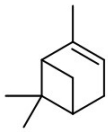	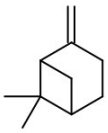	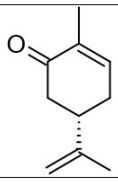	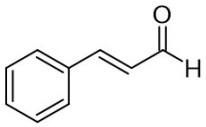
Wax	**Relative polarity**	**Density (g/cm³)**		**Predicted ranking of diffusion speed (fastest to slowest)**				
Paraffin	Least polar	~ 0.900		1	5	3	7	13
Beeswax	Semi-polar	0.921-0.957		2	6	4	8	14
Carnauba	Most polar	0.990-0.999		9	12	11	10	15

CHAPTER TWO: EXPERIMENTAL

Materials

All chemicals and equipment were provided by Western Carolina Universitys Department of Chemistry and Physics. The limonene used was 97% (R)-(+)-limonene from Sigma-Aldrich. The carvone used was 98% l-carvone from Pfaltz and Bauer. The α-pinene used was from Acros Organics and was 98% (S)-(-)-α-pinene. The β-pinene was 94% (-)-β-pinene from TCI. The cinnamaldehyde was from Acros Organics and was 99% trans-cinnamaldehyde. The paraffin wax was from Gulf Wax, the carnauba wax was from VWR, and the beeswax was obtained from a local bee farmer in Cullowhee, NC. The neat IR spectra for each material are available in Figure 1. Because ATR-FTIR was used to collect these spectra, the fingerprint region is visible. The dashed lines in Figure 1 represent the analytical wavelengths for each diffusant.

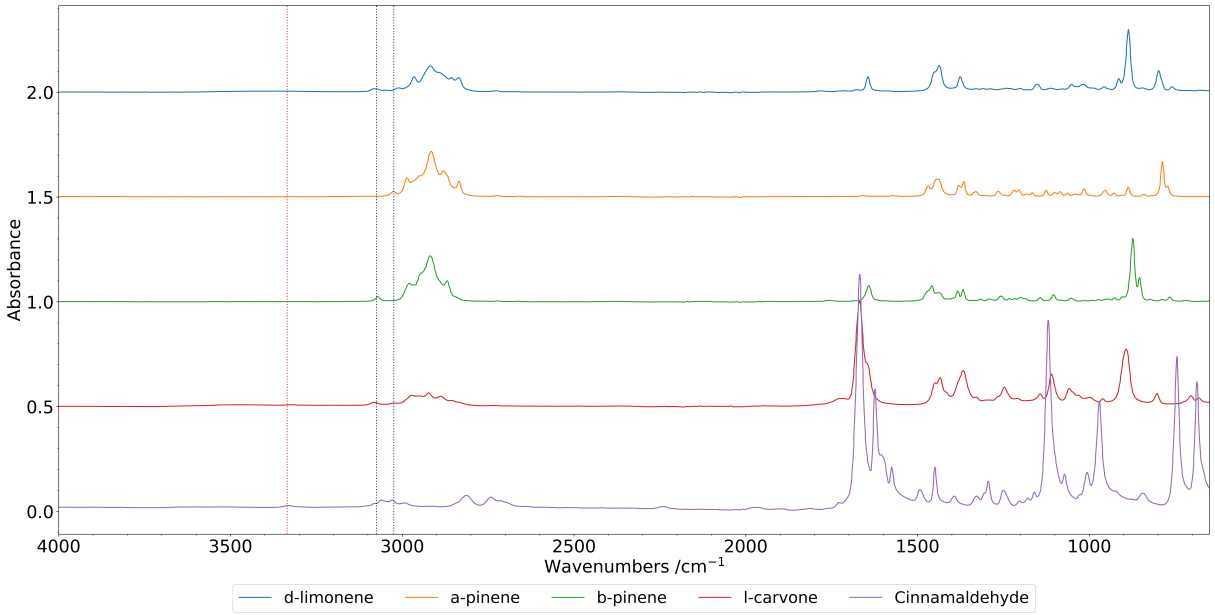

(a) Diffusants

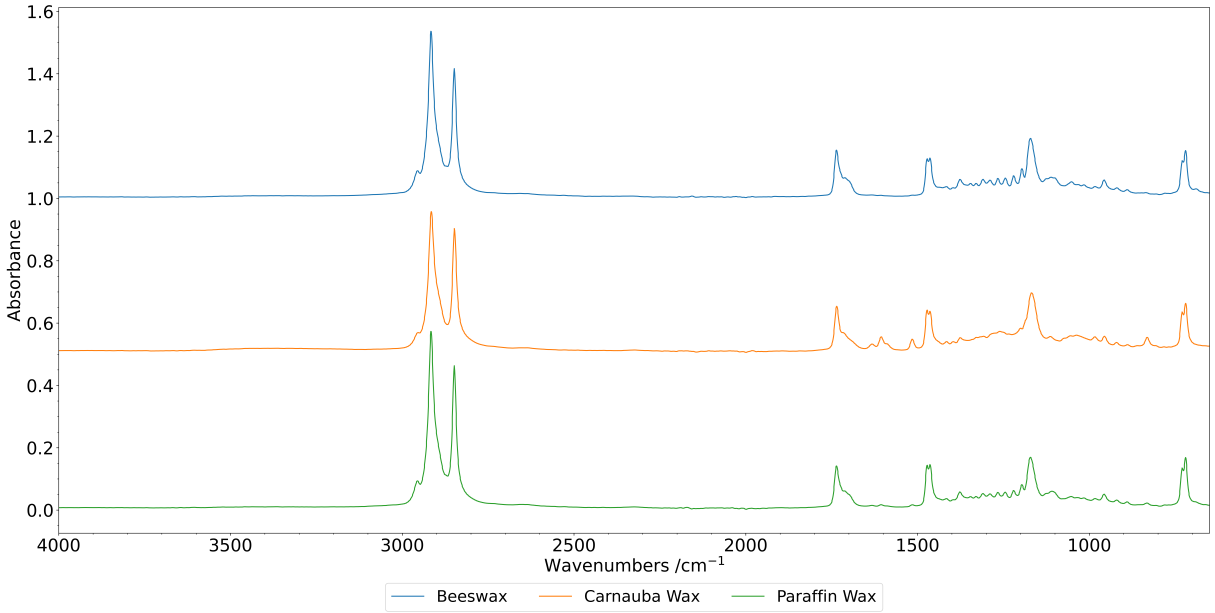

(b) Wax

Figure 1. The neat spectra of the (a) diffusants and (b) waxes used in this experiment. The dashed lines in (a) represent the analytical wavelength for each diffusant, 3075 cm^{-1} for d-limonene, β-pinene, and l-carvone (black), 3025 cm^{-1} for α-pinene (blue), and 3335 cm^{-1} for cinnamaldehyde (red).

Wax Melting Point Determination

The melting point range of each wax was determined using a DigiMelt melting point apparatus from SRS. The ranges were determined to be 57.4-58.2°C for paraffin wax, 64.6-65.1°C for beeswax, and 83.0-84.0°C for carnauba wax. These melting points are tabulated in Table 2.

Diffusion Coefficient Determination

Sample Preparation

Samples for the experiments were created with an emphasis on using low-cost materials. The general design consisted of a small piece of wax sandwiched between two differently-sized panes of glass, shown in Figure 2. These panes of glass were created from microscope slides and were cut using a diamond tip scribe. Nitrile gloves were worn to ensure a clean glass surface and the glass was used as is, except in cases where the glass was observed to be dusty, in which it was wiped with acetone and allowed to dry. The larger glass pane, about 1 inch $\times$ 1 inch, was the bottom of the cell and holds the wax and diffusants in place and the smaller piece of glass, about 0.5 inches $\times$ 1 inch, functions as the top of the cell.

The differently-sized panes of glass are necessary to create a surface to load the diffusant. The waxes were shaped in small, 1 inch $\times$ 1.5 inch rectangular blocks to allow for microtome accessibility. A small piece of wax was cut using a microtome with 25 μm thickness setting to ensure similarly sized slices of wax. The three waxes are tactilely different, and when thinly sliced, the waxes all have different textures so it is difficult to procure completely identical slices of wax. When the paraffin wax is sliced, it rolls up so the rolled wax is placed on the glass directly. The beeswax slices well and yields a flat slice placed directly on the slide. The carnauba wax is brittle and crumbles into a powder-like substance which is placed on the glass.

If the wax slice is simply placed on the glass panes and the top piece of glass is laid on top, the diffusant will travel over or under the wax by capillary action instead of diffusing through the wax. To prevent this non-diffusive travel of diffusants, the wax was placed on the larger piece of glass and melted using a hot plate with a higher heat setting for the carnauba wax and a lower set-

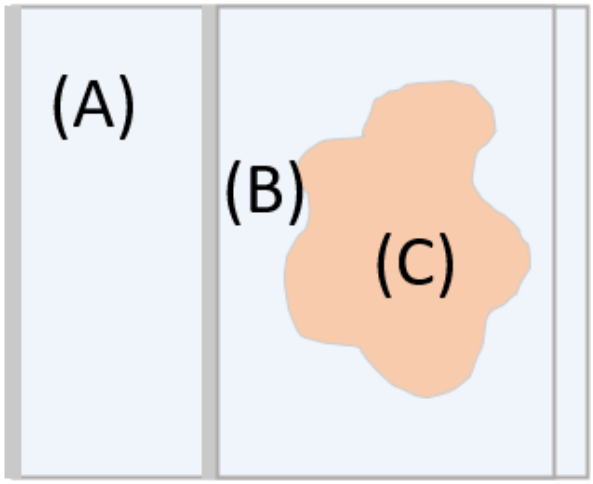

Figure 2. Schematic showing the composition of the sample wax/glass cell. (A) represents the diffusant loading site. (B) represents the reservoir where the diffusant stays during the experiment. (C) represents the melted wax piece.

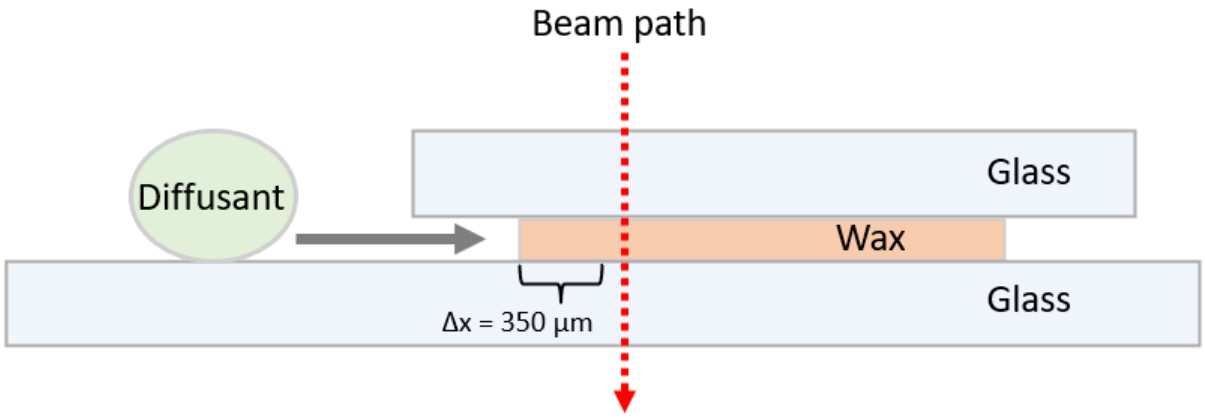

Figure 3. Schematic showing the completed wax cell and IR beam path. Δx represents the lateral distance from the edge of the wax to the beam path.

ting for paraffin wax and beeswax. The second glass piece was heated at the same time to ensure the wax slice did not harden when the top pane was added. The wax was liquid when the two panes of glass were pressed together using light pressure from gloved hands. The resulting wax was roughly centered between the two glass panes. If the wax reached the edge of the top glass pane, the cell was not used.

It is necessary to have space between the glass panes without wax to create a reservoir for the diffusant to reside without being exposed to the air while the diffusant interacts with the wax in the center of the wax/glass cell, shown in (B) in Figure 2. This allows the concentration of diffusant outside the wax to be considered infinite for the duration of the experiment. If the reservoir were absent or not big enough, the concentration of diffusant would decrease by evaporation over the several hours of the experiment; the experiment would not reach equilibrium in this case.

The hardened wax holds the cell together and ensures that the diffusants move through the wax instead of moving above or below the wax slice. The leftover diffusant has a small area to reside in for the duration of the diffusion. These samples were produced about six at a time and stored in a drawer at room temperature until use to ensure protection from dust.

Instrumentation and Setup Procedure

Samples were measured using a Bruker INVENIO FT-IR coupled with a Hyperion 3000 microscope with the instrument parameters shown below in Table 5. Before data collection, the instrument was filled with liquid nitrogen to cool the MCT detector. The wax cell was placed on the microscope stage and the 15x objective was focused using visible light to image the wax between the two glass panes. The instrument was in light transmission mode for these measurements.

Background Spectrum Collection Procedure

A new background was obtained before each sample. This background was obtained by navigating the beam path off of the wax slice and onto the space where the two glass pans overlapped. The double glass background was used to ensure the resulting absorbance spectrum only showed the wax and diffusant. This background was collected as a single beam and saved as a JCAMP-

Table 5. Key instrument parameters.

Parameter	Value
Microscope	Bruker™ Hyperion 3000™
FTIR Spectrometer	Bruker™ INVENIO™
Software	OPUS™ version 9.8.372
Wavelength range	4000–650 cm^{-1}
Near/mid/far IR	Mid
Detector	MCT, Liquid Nitrogen Cooled
Beamsplitter	KBr
Blank	Air
Scans	32
Resolution	8 cm^{-1}

DX file.

Sample Image Collection

Using the OPUS software, a composite image could be collected of the edge of the wax and surrounding areas before and after exposure to the diffusant. These images can show how the diffusants move and change the surfaces of some of the waxes but leave others visibly untouched. The section of the edge of wax was chosen by finding a visually even edge of the wax to ensure even diffusion.

Determination of Wax Thickness

Because the wax is melted before adding the top window to the sample holder, the thickness of the wax was not controlled. Using the microscope coupled to the Bruker INVENIO FT-IR with a 15x objective, the thickness of the wax was determined by vertically observing the very thin gap between the two glass panes of a completed sample cell, assuming that the wax is level between the two panes and the gap is the same thickness as the wax. Visible light was used in reflection mode. The OPUS software images the mobile microscope stage with accompanying stage coordinates given in μm ($\pm$ 0.1) that help determine the size of the gap. Three sample holders with different waxes were observed and the size of the gap was recorded to be from 20.5 to 48.1 μm,

averaged to be 33.3 $\pm$ 13.9 μm. The gap was measured in several different spots and the thickness was consistent throughout for each sample holder.

Sample Spectrum Collection Procedure

After empirically testing different lateral depths into the wax, the ideal point for measurement was found to be about 350 μm laterally from the edge of the wax. This distance is determined by using the given coordinates from the microscope stage. The beam path was positioned over the edge of the wax and the coordinates, given in micrometers, were recorded. Adding 350 μm to the x coordinate and navigating the beam path to the new x coordinate allowed the measurement to be taken in the ideal spot. This set-up is represented by Figure 3. A repeated measurement was set up for each sample after background collection and the beam path appropriately placed. The OPUS program can automatically take measurements between set periods of time. For these measurements, there were a variable number of single beam measurements, usually ranging from thirty to fifty measurements, taken seven minutes (420 seconds) apart. The first four measurements were taken before the introduction of diffusant to establish an absorbance baseline corresponding to t = 0. Twenty-one minutes into the data collection, which is equivalent to four measurements, 8 μL of diffusant was introduced with a 10 μL syringe by placing the liquid on the outlying surface on the bottom glass pane. As the diffusant penetrated the wax, there was a new spectral measurement every seven minutes, resulting in single beam, time-sensitive spectra, saved as JCAMP-DX files.

Data Processing

The single beam spectra were processed using Python 3 v12.0. The repeated measurements were loaded into a header file and transformed into an absorbance spectrum using the single beam double glass background. The spectral data was cropped and baseline corrected from 2600 to 3200 cm^{-1} to exclude the glass absorbance and to focus on the diffusant band. An analytical wavelength for each diffusant was chosen: 3075 cm^{-1} for d-limonene, β-pinene, and l-carvone, 3025 cm^{-1} for α-pinene, and 3335 cm^{-1} for cinnamaldehyde, shown in Table 3. In unsuccessful sys-

tems, the diffusant band did not change over time and this data was deemed unusable. If the diffusant band changed over time, the absorbance at the analytical wavelength was plotted verses time to give a profile of the increasing absorbance, and by proxy, concentration, for each system. The absorbance was normalized to the maximum absorbance at the analytical wavelength. The resulting curve was sigmoidal in nature. The first four points before the addition of diffusant purposely establish a zero diffusant baseline absorbance and were followed by an increase in absorbance as the diffusant started to interact with the wax. The most linear portion of the curve was used to determine the D of each system. The linear points were chosen by identifying the inflection point of the curve and indexing three points on either side of the inflection point to create a six point curve. This data was fit using the method of least squares provided by the NumPy Python library with the function polyfit.[36] The slope from this linear fit was used to calculate D for the system. The error for this result was determined by error propagation for each individual system, using 0.1 μm error for the Δx parameter from the associated microscope stage, and the linear regression error associated with the calculated slope. For replicate measurements of the system, each D were averaged and the error presented is the standard deviation of those measurements.

Solvation Test

Experiment Preparation and Data Collection

Some of the systems did not show any diffusion over the duration of the experiment. This unsuccessful systems were analyzed with a qualitative solvation test to determine if the diffusant would interact with the wax outside of the five-hour time frame of the diffusion experiment. Using a well plate, a small amount of wax was placed in each well and diffusant was added. The plate was covered and left overnight. The next day, the diffusant was analyzed using ATR-FTIR with the parameters in Table 6. A single background was collected at the beginning of the diffusant analysis. The diffusants were pipetted directly onto the ATR crystal and the IR spectrum was collected. The spectra were saved as single beam JCAMP-DX files and the neat diffusant spectra

were subtracted from the resulting spectra to yield a difference spectrum.

$$\text{Difference absorbance} = [\text{Wax + diffusant absorbance}] - [\text{Diffusant absorbance}] \quad (7)$$

These difference spectra can show new IR bands that are present in the diffusion spectra but not in the neat spectra; these new bands are marked with positive absorbance. The presence of positive peaks indicate the solvation of the wax by diffusant and could suggest eventual diffusion

Table 6. Solvation test instrument parameters.

Parameter	**Value**
ATR	SmartiTX™
FTIR Spectrometer	Nicolet™ IS™ 10
Software	OMNIC™ version 9.8.372
Wavelength range	4000–650 cm^{-1}
Near/mid/far IR	Mid
Detector	MCT/A
Beamsplitter	KBr
Blank	Air
Scans	32
Resolution	8 cm^{-1}

CHAPTER THREE: RESULTS AND DISCUSSION

Broad Overview

Visual images were collected of each system before and after the measurements. An example image is shown in Figure 4. The raw spectra for each timed measurement were overlaid. The number of spectra varied for each experiment, but stayed between 30-50 spectra. The diffusion process occurs in the first twenty measurements and the rest of the data collection was to establish an equilibrium line. The region from 650-2200 cm^{-1} is marked with no absorbance because the glass used in the wax cell absorbs the IR light. For each system, the raw spectra were cropped to 2600-3200 cm^{-1} to focus on the wide C-H stretching band and the analytical wavelengths. An example cropped overlaid spectra is shown in Figure 5.

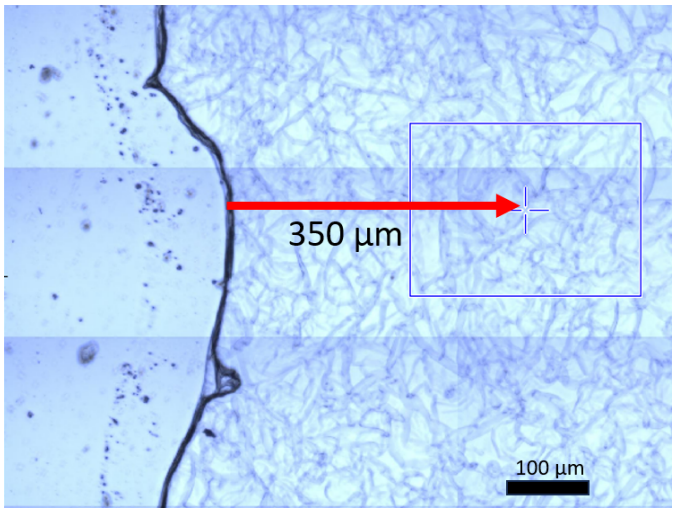

Figure 4. An example composite image of the wax edge. The red arrow represents the path of the diffusant.

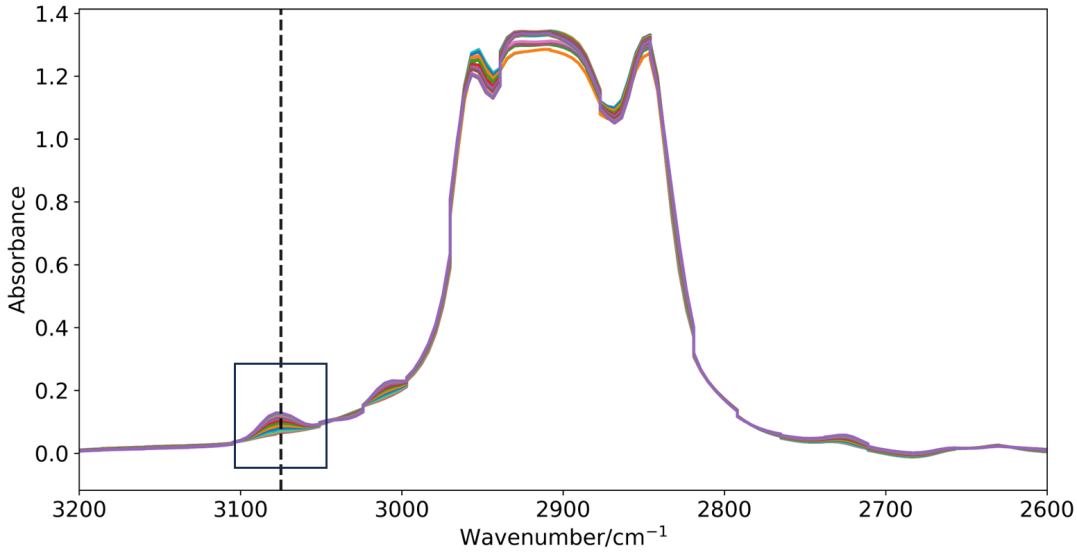

Figure 5. d-Limonene and paraffin wax overlaid cropped spectra. The diffusant band is boxed. The dashed line represents the analytical wavelength, 3075 cm^{-1}.

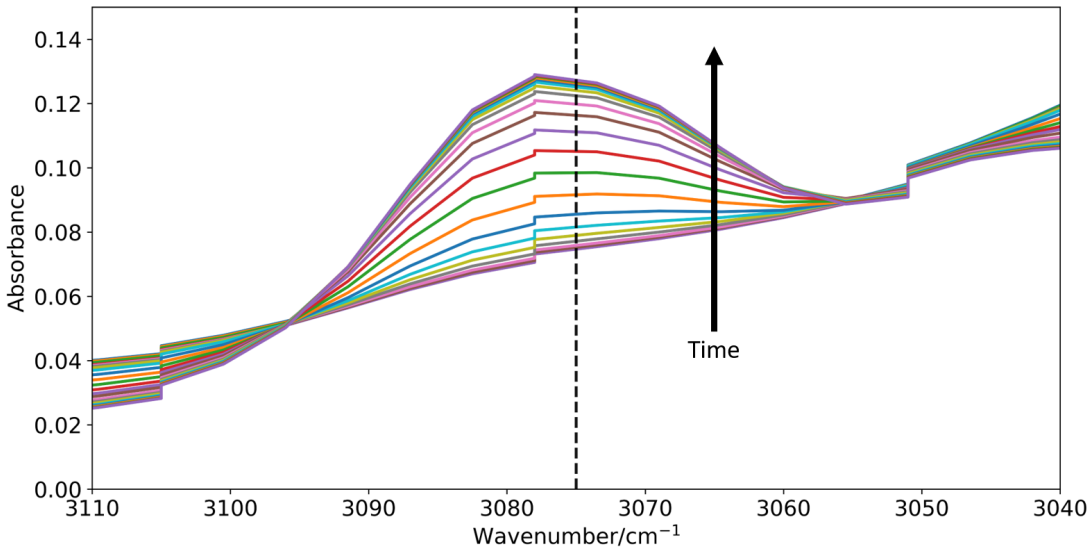

Figure 6. d-Limonene and paraffin wax diffusant band. The dashed line represents the analytical wavelength, 3075 cm^{-1}.

An example overlaid spectral band at the analytical wavelength is shown in Figure 6. There are vertical jumps in absorbance at 3105, 3077, 3051 cm^{-1} that are an artifact of the data processing program. The absorbance values at this wavelength for each measurement were normalized to the absorbance maximum and plotted verses time which yielded a diffusion profile, shown in Figure 7. The most linear points of diffusion were chosen around the inflection point and are highlighted in orange. The absorbance values of these six points were plotted versus $\sqrt{t}$, shown in Figure 8. The slope of this line, $\left(\frac{2}{\Delta x}\sqrt{\frac{D}{\pi}}\right)$, is used to determine D of the system. D values are given in $\mu m^2/s$.

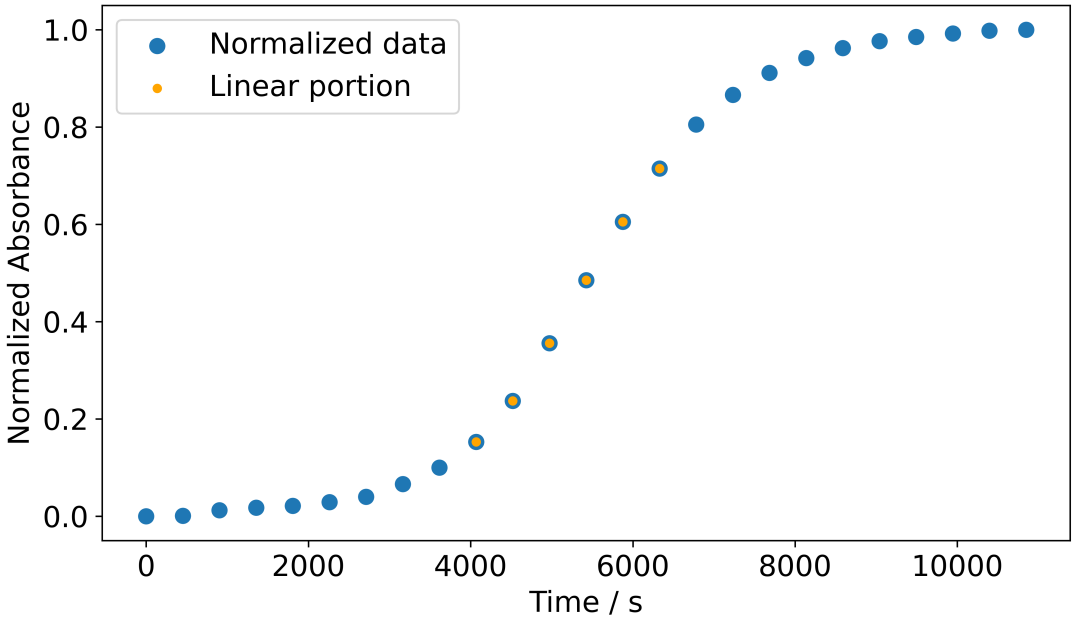

Figure 7. The diffusion profile for one of the limonene/paraffin wax systems. Data selected for calculating D are shown in orange.

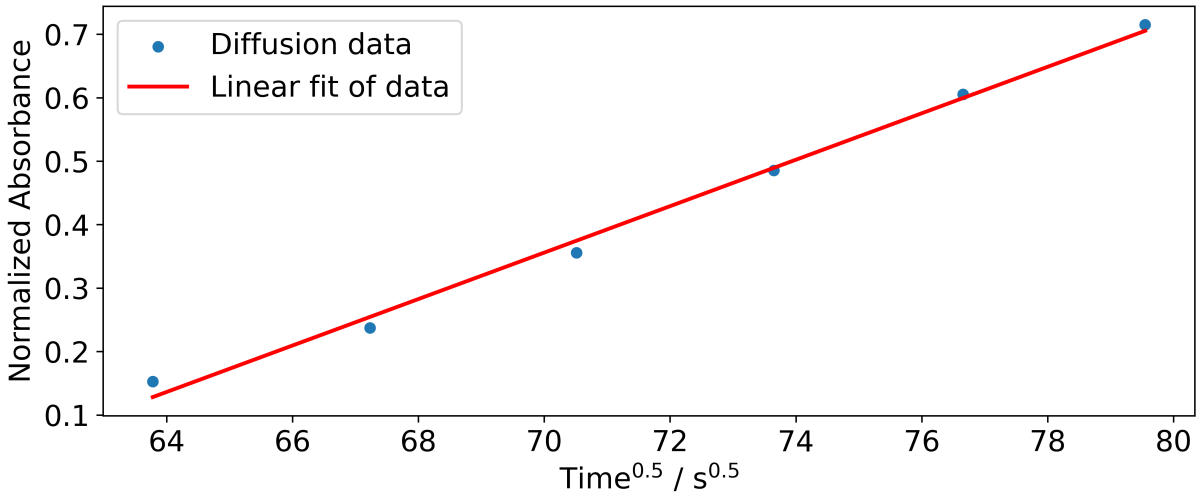

Figure 8. The linear fit of the selected points from the diffusion profile of the limonene/paraffin wax systems.

Diffusion Experiment Results

Data Collection Success Discussion

The method development nature of this project contributed to low data success; a large number of measurements were characterized by a lack of measured diffusion. Among these measurements were the unsuccessful systems that did not exhibit any diffusive activity over the measurement time frame. The unsuccessful systems were those involving l-carvone, cinnamaldehyde, and carnauba wax. Several avenues were explored to try and alter conditions of the experiment, including decreasing the Δx from 350 to 50 µm and increasing the time of experiment from five up to eight hours. The experiments with these new conditions were still marked by no measured diffusion.

Sample preparation also introduced error into these experiments. The thickness of wax was found to range from 20.5 to 48.1 µm, so the thickness of the wax could vary up to 200%. There could also be defects in the wax layer that could lead to uneven diffusion from sample to sample, such as the wax not being flush between the two panes so the diffusant could move on top or be-

low the wax layer and diffuse into two directions. Variation in samples could have contributed to low data success.

Due to time constraint and instrumentation issues, only two systems have a triplicate data set: d-limonene/paraffin wax and α-pinene/beeswax. Three other systems have two replicates: d-limonene/beeswax, α-pinene/paraffin wax, and β-pinene/beeswax. One measurement for α-pinene/paraffin wax was excluded from this analysis because the data was collected right before the instrument used underwent maintenance and the resulting data does not accurately describe the diffusion process of this system. Unfortunately, only one set of spectral data was collected for the β-pinene/paraffin wax system, so both this system and the α-pinene/paraffin wax system have only one data set used in calculation of D. The errors for these two sets are those propagated from the D calculation.

Images of Systems

Composite images were obtained of each system using the microscope coupled to the Bruker INVENIO FT-IR (Figures 9-11). These images show the left side of the wax between the two glass panes and the reservoir where the diffusant resided during the experiment. The lighter area is the reservoir and the darker, textured area corresponds to the wax. The beam path is represented by the crosshair of the microscope cursor. The images of the successful paraffin wax systems are shown in Figure 9 and the successful beeswax systems are shown in Figure 10. An image of carnauba wax exposed to limonene for the duration of the experiment is included in Figure 11 to illustrate the lack of visual interaction in the unsuccessful systems.

The successful systems were able to dissolve some of the edge of the wax. Note in the "after" pictures the edge of the wax has a changed surface. In the α-pinene and paraffin wax imaging (Figure 9), the edge of the wax moved during the experiment and a faint line in the "after" picture represented where the edge of the wax was located. In all successful systems, the paraffin wax seemed to visually be more dissolved than the beeswax.

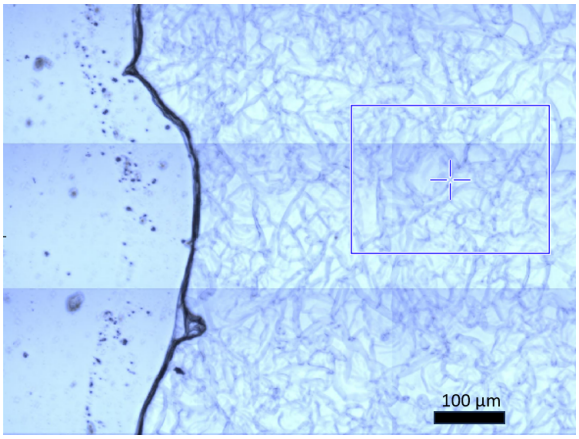

d-limonene/paraffin, before

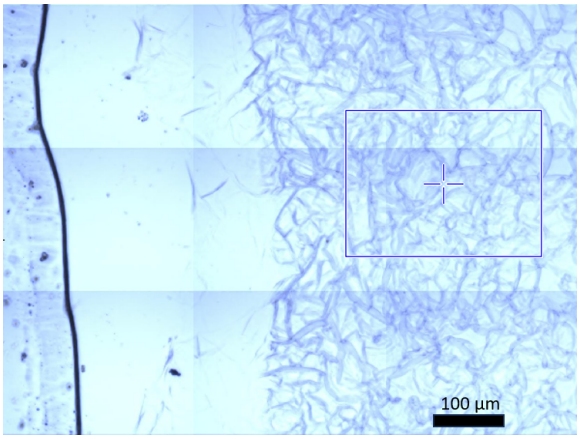

d-limonene/paraffin, after

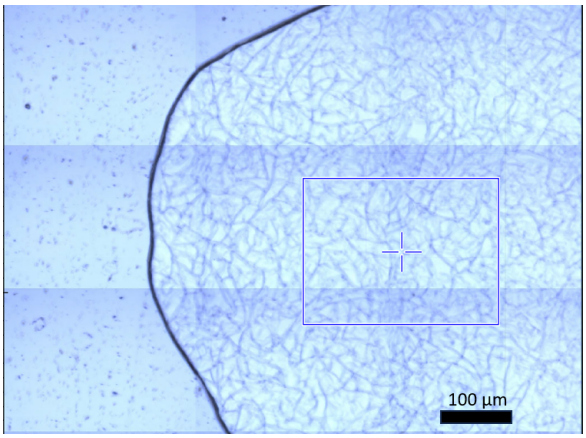

α-pinene/paraffin, before

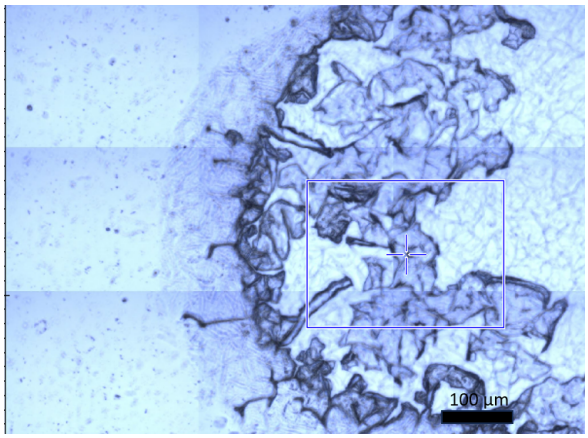

α-pinene/paraffin, after

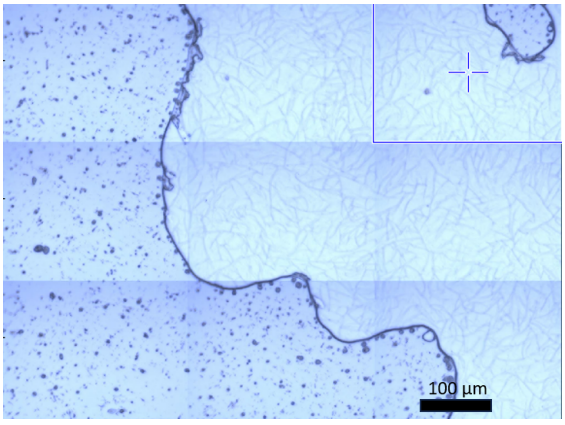

β-pinene/paraffin, before

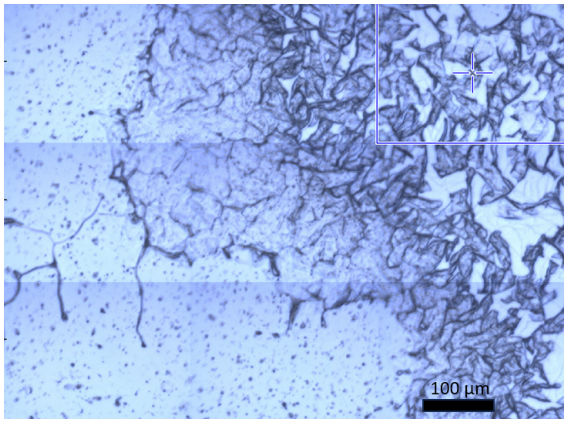

β-pinene/paraffin, after

Figure 9. Images collected of each successful paraffin wax system.

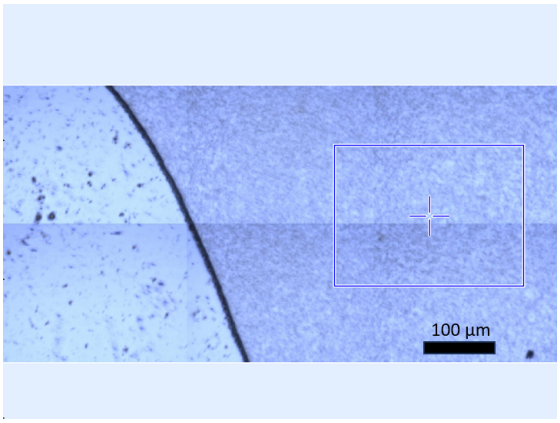

d-limonene/beeswax, before

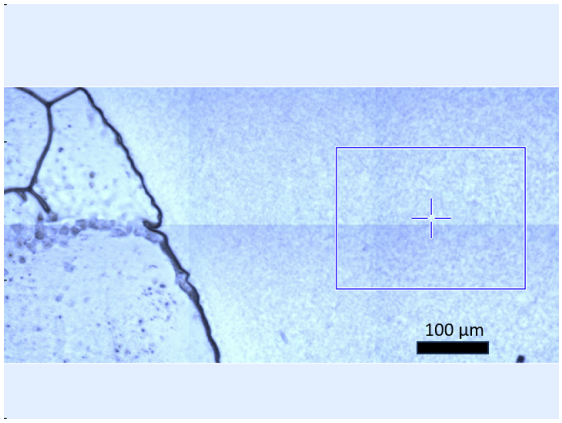

d-limonene/beeswax, after

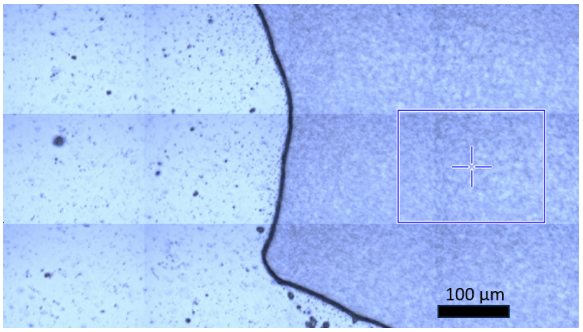

α-pinene/beeswax, before

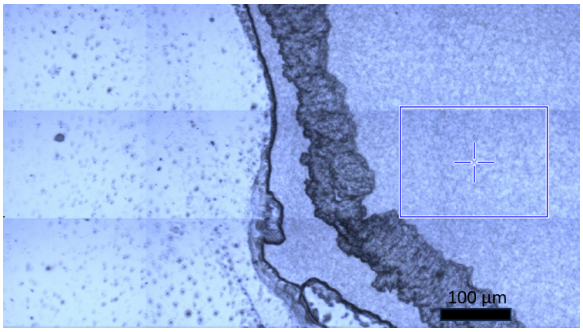

α-pinene/beeswax, after

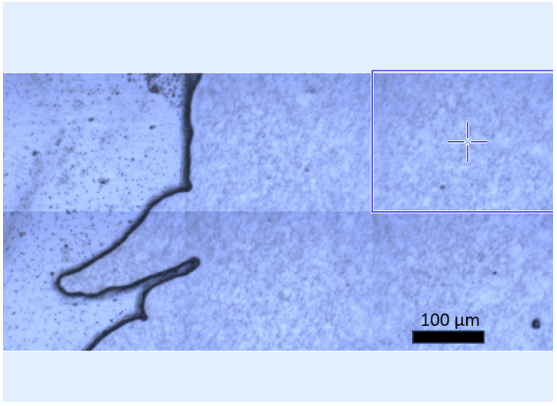

β-pinene/beeswax, before

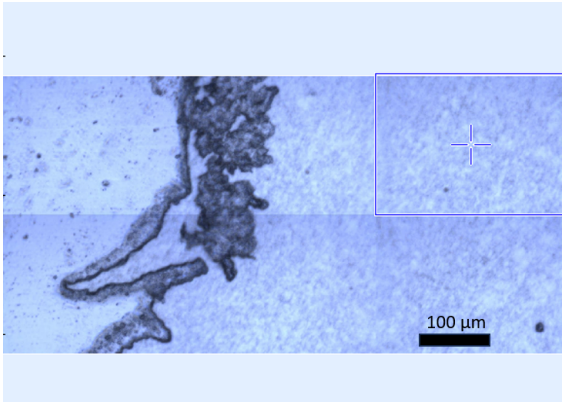

β-pinene/beeswax, after

Figure 10. Images collected of each successful beeswax system.

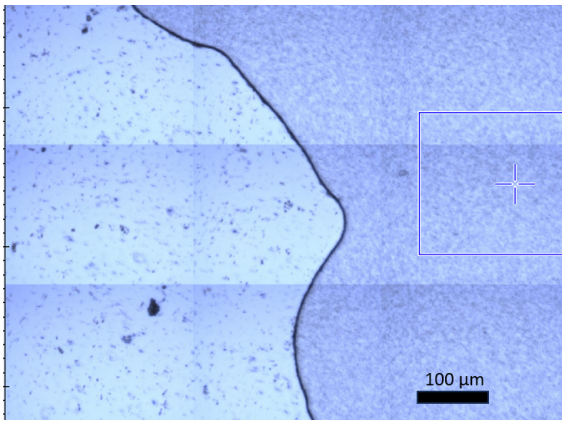

d-limonene/carnauba, before

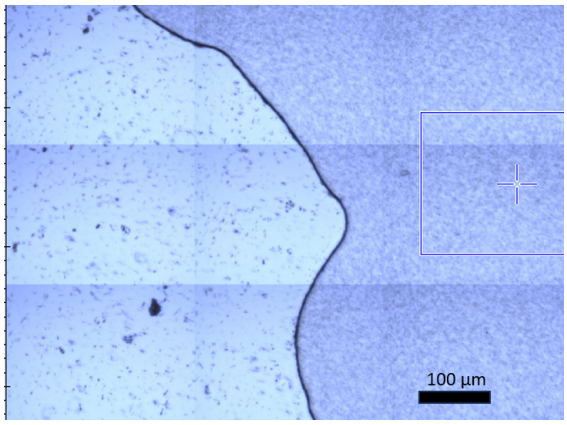

d-limonene/carnauba, after

Figure 11. An image collected of the d-limonene and carnauba system before and after addition of d-limonene.

Diffusion Coefficients by System

Table 7 holds the determined diffusion coefficients and slopes of linear fit by system. The average diffusion coefficients by system are tabulated in Table 8. The errors associated with each individual D by system are propagated from the error in the determined slope and the error associated with Δx. The average D error is the standard deviation of the measurements, except for the pinene/paraffin systems, where the error is still propagated. The average D by each system are charted in Figure 12. The sample size for the measurements in this experiment are small and the standard deviations for these measurements are large, represented by the error bars in Figure 12. The overlaid normalized diffusion profiles for each system can be found in Figure 13.

There are a wide range of values for D for each system and a larger sample size is needed to draw definite conclusions about the behavior of each diffusant in each wax. Plotting each diffusion profile on the same graph (Figure 13) shows two clusters of measurements corresponding to the different wax systems. Paraffin wax systems reach a maximum absorbance later than the beeswax systems, indicated by the horizontal shift in the profiles. Although there is not enough data for any system to draw any definite conclusions in difference of behavior, the clustering of

Table 7. Tabulated values from the linear fitting of initial diffusion data by system.

System	**Trial**	**Slope ($s^{-1/2}$)**	**R^2**	**D (μm^2 / s)**
d-limonene/paraffin	1	0.0259 ± 0.0005	0.9987	64.713 ± 0.006
d-limonene/paraffin	2	0.037 ± 0.005	0.9940	128.903 ± 0.007
d-limonene/paraffin	3	0.0300 ± 0.0004	0.9993	86.677 ± 0.004
d-limonene/beeswax	1	0.025 ± 0.002	0.9865	62.51 ± 0.01
d-limonene/beeswax	2	0.0301 ± 0.0009	0.9970	87.218 ± 0.006
α-pinene/paraffin	1	0.0282 ± 0.0004	0.9992	76.379 ± 0.005
α-pinene/beeswax	1	0.0191 ± 0.0008	0.9936	35.18 ± 0.01
α-pinene/peeswax	2	0.032 ± 0.002	0.9804	97.21 ± 0.01
α-pinene/beeswax	3	0.037 ± 0.001	0.9955	128.240 ± 0.006
β-pinene/paraffin	1	0.0212 ± 0.0002	0.9996	45.571 ± 0.005
β-pinene/beeswax	1	0.0341 ± 0.0007	0.9985	111.974 ± 0.004
β-pinene/beeswax	2	0.029 ± 0.002	0.9751	80.80 ± 0.02

Table 8. Average D (μm^2 / s) by system with standard deviation. *Propagated error.

	Paraffin Wax	**Beeswax**	**Carnauba Wax**
d-limonene	93.4 ± 32.6	74.9 ± 17.5	-
α-pinene	76.379 ± 0.005*	86.9 ± 47.4	-
β-pinene	45.571 ± 0.005*	96.4 ± 22.0	-
l-carvone	-	-	-
Cinnamaldehyde	-	-	-

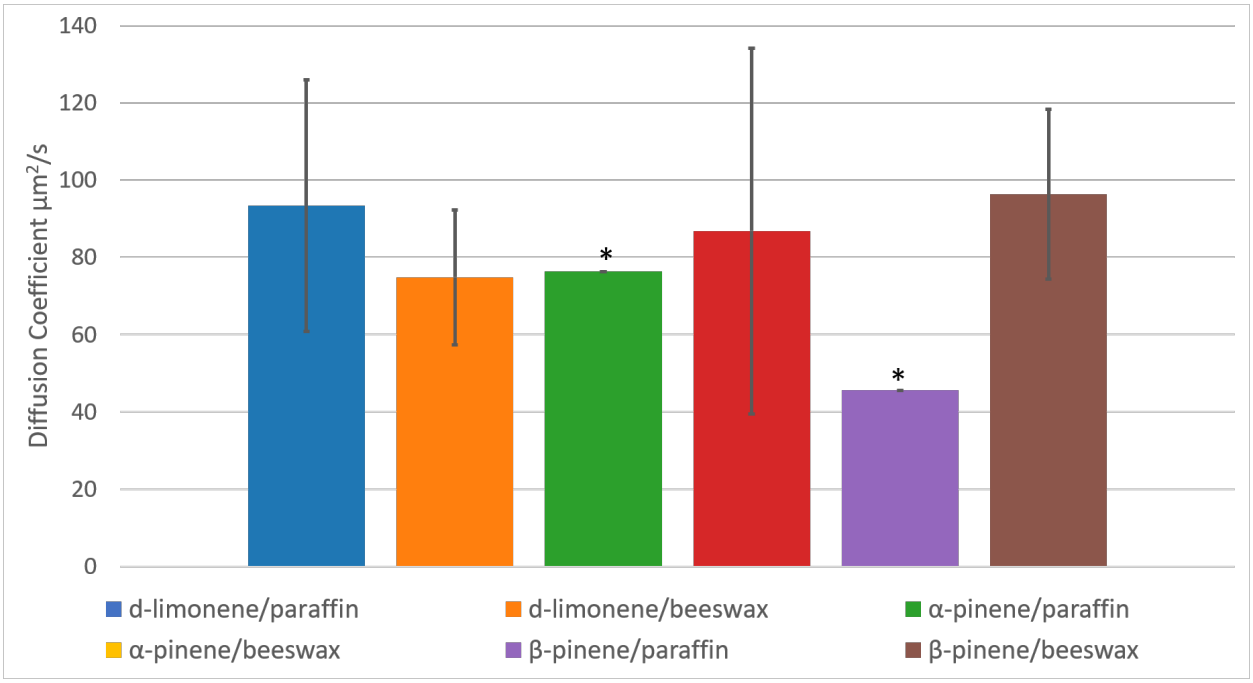

Figure 12. Average D by system. *These data sets have only one measurement.

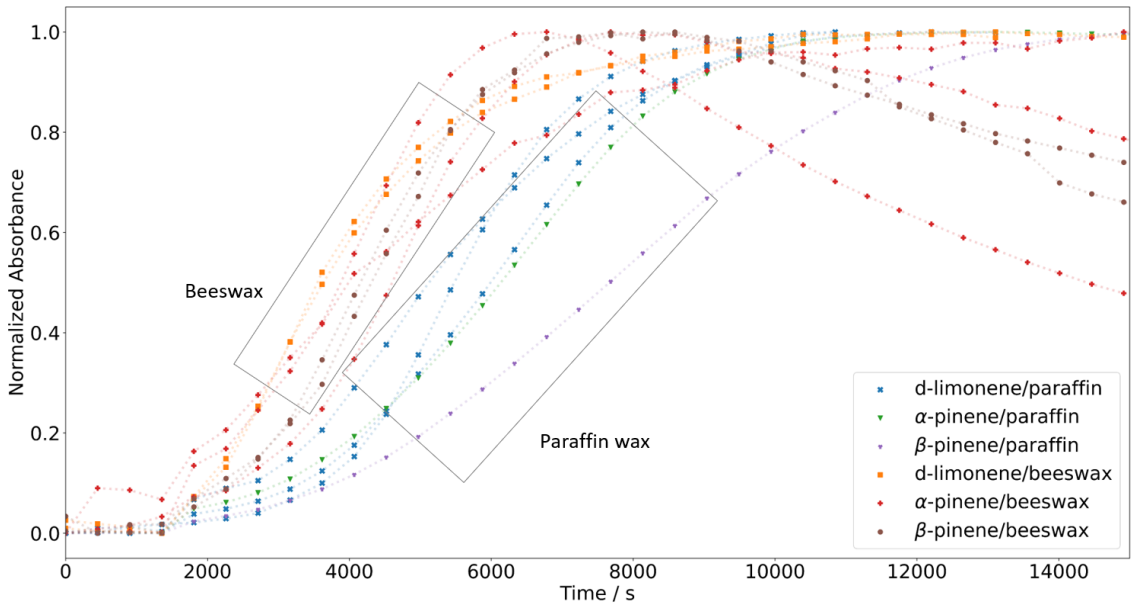

Figure 13. The overlaid diffusion profiles for each experiment. The boxes surround the clusters of diffusion profiles by wax.

data by wax suggests that there is a difference in the diffusivity of paraffin wax and beeswax systems.

Beeswax is a more polar wax (67% saturated hydrocarbons) than paraffin wax ($\sim$ 100% saturated hydrocarbons). A slower absorbance maximum observed in the paraffin wax could indicate that the three diffusants, all nonpolar, are interacting intermolecularly more in the paraffin wax than in the beeswax systems. The images of the beeswax and paraffin systems, Figures 9-10, also could indicate increased interaction in the form of solvation between the diffusants and paraffin wax. The concentration of saturated hydrocarbons in the paraffin wax could be preventing the diffusants from reaching equilibrium as quickly as in the beeswax. On a physical front, the saturated hydrocarbons in paraffin wax could be nestled together and not leave as much room for the diffusants to move through as the oxygenated beeswax. The presence of esters, fatty acids, and unsaturated hydrocarbons in the composition of beeswax could allow the nonpolar diffusants to move through the matrix of molecules more effectively than in the paraffin wax, despite the beeswax being more dense than paraffin wax.

Solvation Test

A qualitative solvation test was conducted to see if given enough time, the unsuccessful diffusants, l-carvone and cinnamaldehyde, would interact with the waxes, and if carnauba wax would interact with any of the diffusants. The diffusants and small pieces of wax were allowed to interact overnight and the following day, the IR spectrum of each of the diffusants were collected. Using Equation 7, the neat diffusant spectra were subtracted from the wax-exposed spectra to yield difference spectra. The resulting absorbance values were normalized to the maximum absorbance then cropped from 2600-3200 cm^{-1}. The difference spectra for each wax are overlaid with the respective wax in Figures 14-16.

As expected, d-limonene and the pinenes were able to dissolve paraffin and beeswax, suggested both visually and spectroscopically. These diffusants completely visually dissolved paraffin wax and beeswax and there are wax C-H stretching bands present in the difference spectra in

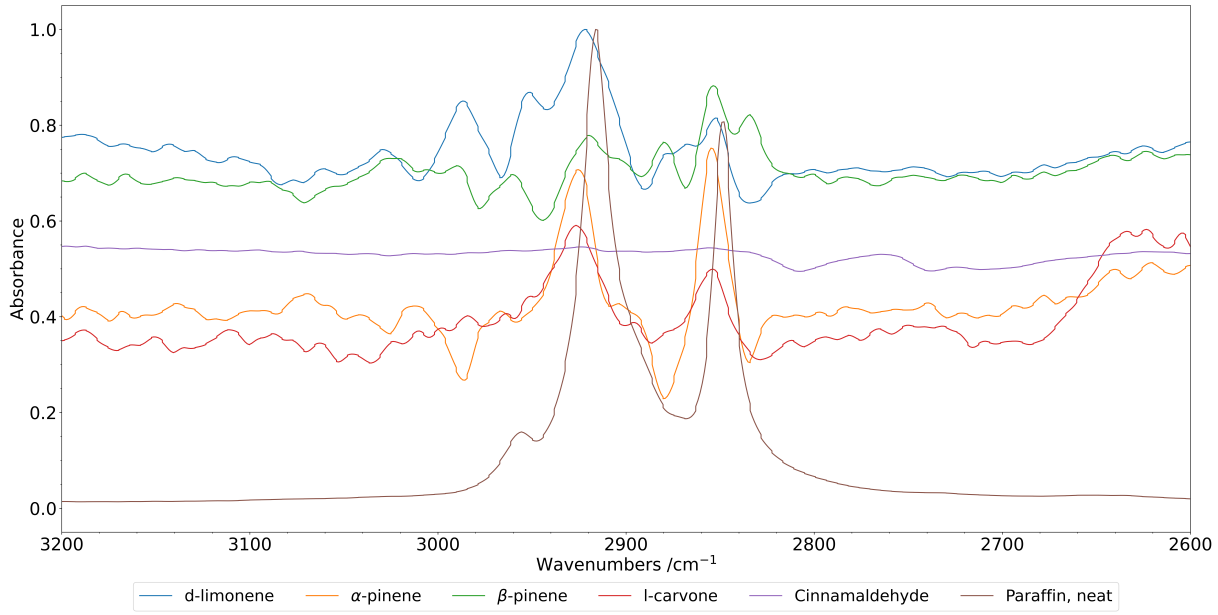

Figure 14. The difference spectra of each diffusant and paraffin wax compared to the neat spectrum of paraffin wax.

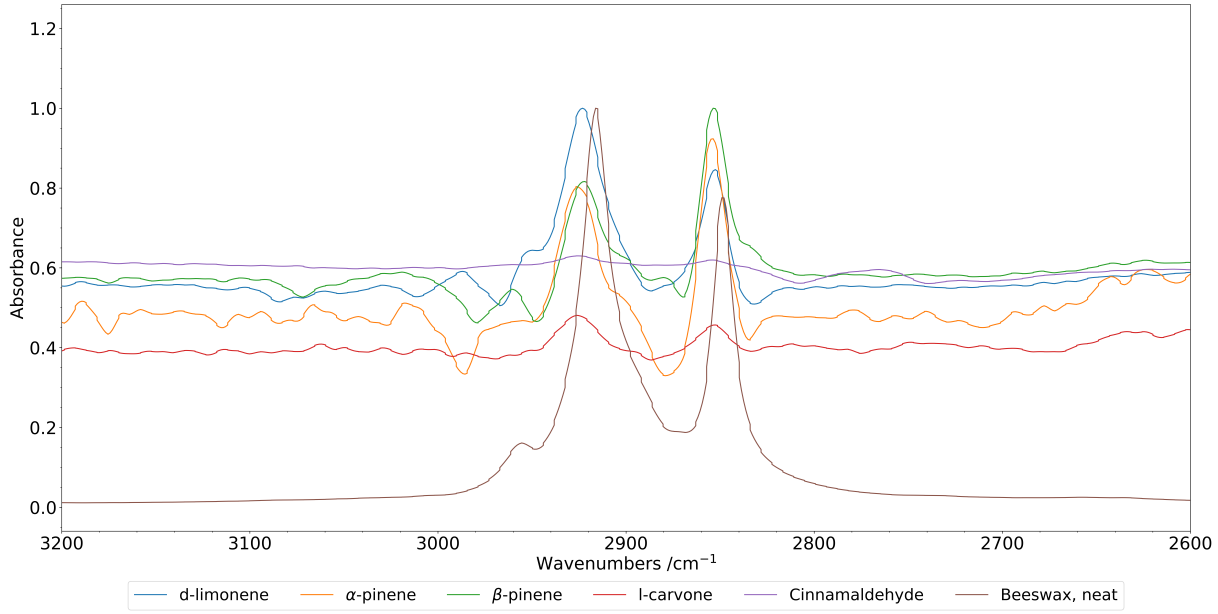

Figure 15. The difference spectra of each diffusant and beeswax compared to the neat spectrum of beeswax.

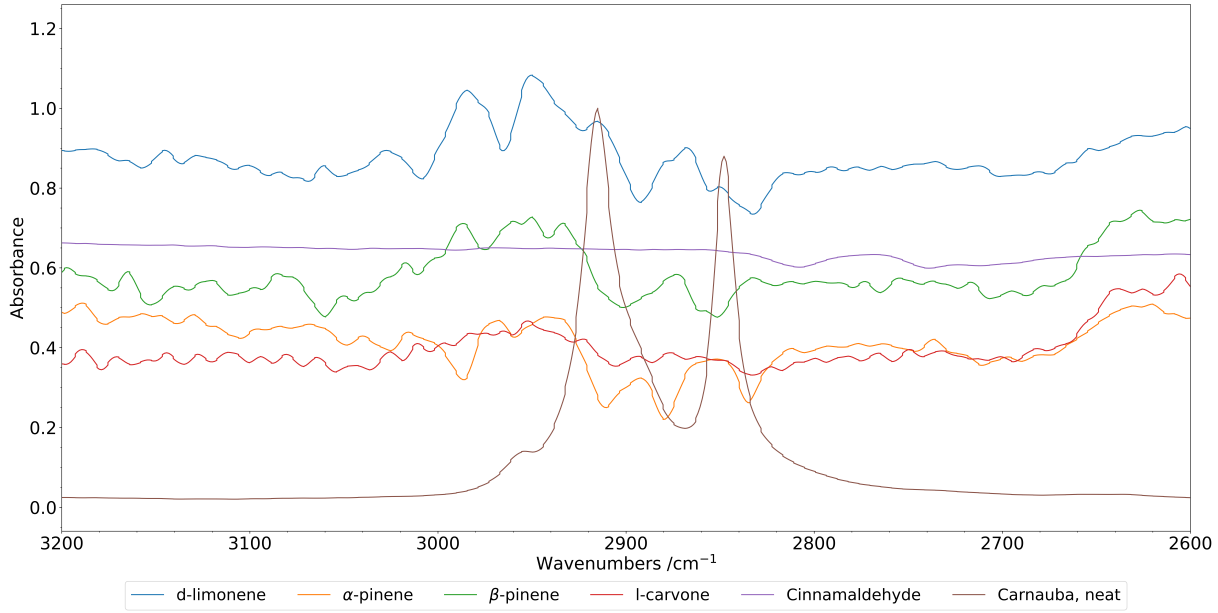

Figure 16. The difference spectra of each diffusant and carnauba wax compared to the neat spectrum of carnauba wax.

Figures 14 and 15. The difference spectra for paraffin wax and beeswax also shows wax bands present in l-carvone, despite the lack of visual solvation. These bands are smaller than the d-limonene and pinene bands, suggesting interaction to a lesser extent. Because the structures of carvone and limonene are similar save for a ketone, it can be concluded that the polar ketone group present on carvone prevents the measurement of diffusion into wax under the conditions presented here. l-carvone was not able to dissolve the carnuaba wax during this time period, indicated by the lack of wax bands in the l-carvone/carnauba wax difference spectrum (Figure 16).

Cinnamaldehyde was not able to dissolve the paraffin wax and beeswax, but did interact with the waxes, as evident from the bands located at around 1100 and 1700 cm^{-1} shown in Figure 17. The negative/positive shape of these bands could indicate the shift of a band, suggesting interaction of some kind between cinnamaldehyde and each wax. Cinnamaldehyde also has a polar functional group, but unlike carvone, it was not able to dissolve the beeswax and paraffin wax. Carvone is a flexible molecule compared to the ring-locked cinnamaldehyde and perhaps it is this

flexibility that allows carvone to dissolve the wax.

Carnauba wax was unable to be visually dissolved by any of the diffusants. There are very small bands in the C-H stretching region for d-limonene and α-pinene, but there are no bands for β-pinene, l-carvone, and cinnamaldehyde. The bands for d-limonene and α-pinene are too small to conclude definite interaction. The bands around 1100 and 1700 cm^{-1} are still present for cinnamaldehyde and are the largest in carnuaba wax (Figure 17). This could indicate increased interaction between cinnamaldehyde and carnuaba wax compared to the other waxes. Carnauba wax is the densest and most polar wax (1% saturated hydrocarbons) and so polar interactions between cinnamaldehyde could occur. There were no such observed interactions between carvone and carnuaba wax, so perhaps the ketone in carvone is less accessible for molecular interaction than cinnamaldehyde due to the position of the oxygen (middle versus end of the molecule).

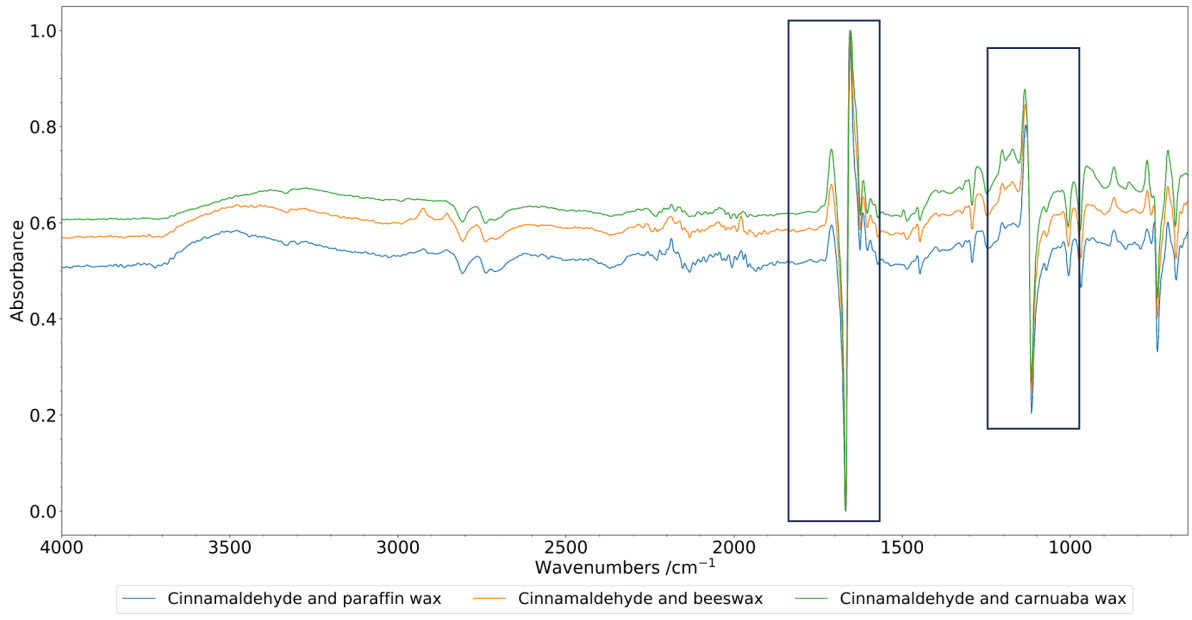

Figure 17. The overlaid full difference spectra of cinnamaldehyde and each wax. The spectral areas of interaction are boxed.

The solvation test indicates that given a longer time frame, l-carvone will interact with paraffin and beeswax, making diffusion of these systems possible. d-limonene and α-pinene interacted very little with carnauba wax but perhaps a longer diffusion time frame would increase interaction. β-pinene, l-carvone, and cinnamaldehyde did not interact with carnauba wax over this time period. Cinnamaldehdye did not dissolve any of the waxes, but could possibly interact with them over a given period of time.

CHAPTER FOUR: CONCLUSION

Table 9. Hypothesis table detailed with characterization for each system.

			Diffusant	d-limonene	α-pinene	β-pinene	l-carvone	Cinnamaldehyde
			Relative polarity	Nonpolar	Nonpolar	Nonpolar	Semi-polar	Most polar
			Relative flexibility	Most flexible	Slightly flexible	Slightly flexible	Semi-flexible	Least flexible
			Structure	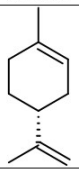	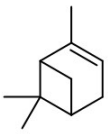	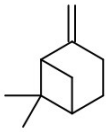	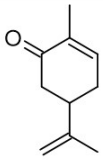	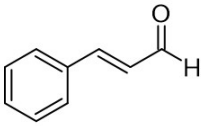
Wax	**Relative polarity**	**Density (g/cm³)**		**Average diffusion coefficients (μm²/s)**				
Paraffin	Least polar	~ 0.900		93.4±32.6	76.379 ±0.005	45.571 ±0.005	Solvation measured	No measured solvation
Beeswax	Semi-polar	0.921-0.957		74.9±17.5	86.9±47.4	96.4±22.0	Solvation measured	No measured solvation
Carnauba	Most polar	0.990-0.999		No measured solvation	No measured solvation	No measured solvation	No measured solvation	No measured solvation

The table from the hypothesis is filled with characteristics for each system in Table 9. The methods presented are a novel path to determining the diffusivity of a solid-liquid system by using micro-FTIR. There were six successful systems for the diffusion experiment described: d-limonene and paraffin wax, d-limonene and beeswax, α-pinene and paraffin wax, α-pinene and beeswax, β-pinene and paraffin wax, and finally β-pinene and beeswax. There was no measured diffusion in the experiment duration for l-carvone and cinnamaldehyde in any of the three waxes. Polar functional groups may prevent l-carvone from diffusing through the wax. No diffusion was measured in the experiment duration for any carnauba wax system, which could be due to its polarity and density.

The determined diffusion coefficients of the successful systems showed no clear differences

between the rates of diffusion from system to system. There were large standard deviations in the measurements due to small sample size; factoring this in, each diffusion coefficient was too similar to draw any conclusions about individual diffusant behavior. There was an observed clustering of diffusion profiles by wax, indicating some diffusivity difference between paraffin and beeswax. These differences are likely attributed to the chemical composition of the waxes. Beeswax systems reached an equilibrium at maximum absorbance more quickly than paraffin wax systems despite being more dense and having higher oxygen content.

The qualitative solvation test showed that d-limonene and the pinenes visually dissolved paraffin and beeswax. There were C-H stretching bands corresponding to wax in these difference spectra. l-carvone did not visually dissolve paraffin or beeswax, but there were wax bands present in the difference spectra, suggesting interaction over a longer period of time. Cinnamaldehyde did not dissolve any of the waxes, nor were any wax bands present in the spectra. Carnauba wax was not dissolved by any of the diffusants and no carnauba wax bands were present in any diffusant spectra.

The standard deviation of each averaged D was large for all of the systems, so in future work the sample size for each system should be increased. Using a different sample holder besides glass could allow access to the fingerprint region of the IR spectrum which could contain valuable information on how the wax and diffusant interact. Also, standardizing the sample holder could help minimize error in diffusion coefficient determination. Wax was used as an imitation of the mosquito exoskeleton cement and by altering the wax or replacing it with substrate to make it more akin to cement, this method could be better applied to studying the diffusion of insecticide across the arthropod exoskeleton. Ultimately, this method is a relatively inexpensive method for determining the diffusivity of a system and could be applied to nearly any system in need of diffusion characterization after more development.

REFERENCES

[1] WHO: The World Malaria Report. 2022.

[2] Xu, Y.; Xu, J.; Zhou, Y.; Li, X.; Meng, Y.; Ma, L.; Zhou, D.; Shen, B.; Sun, Y.; Zhu, C. CPR63 promotes pyrethroid resistance by increasing cuticle thickness in *Culex pipiens pallens*. *Parasites & Vectors* **2022**, *15*, 1–7.

[3] Ranson, H.; Guessan, R.; Lines, J.; Moiroux, N.; Nkuni, Z.; Corbel, V. Pyrethroid resistance in African anopheline mosquitoes: what are the implications for malaria control? *Trends in Parasitology* **2011**, *27*, 91–98.

[4] Center for Disease Control Mosquito Control. https://www.cdc.gov/mosquitoes/mosquito-control/index.html, Accessed: 2023-05-06.

[5] Vincent, J. F.; Wegst, U. G. Design and mechanical properties of insect cuticle. *Arthropod Structure & Development* **2004**, *33*, 187–199.

[6] Norris, E. J.; Bloomquist, J. R. Co-Toxicity factor analysis reveals numerous plant essential oils are synergists of natural pyrethrins against *Aedes aegypti* mosquitoes. *Insects* **2021**, *12*, 154.

[7] Dang, K.; Doggett, S. L.; Veera Singham, G.; Lee, C.-Y. Insecticide resistance and resistance mechanisms in bed bugs. *Parasites & Vectors* **2017**, *10*, 1–31.

[8] Wood, O.; Hanrahan, S.; Coetzee, M.; Koekemoer, L.; Brooke, B. Cuticle thickening associated with pyrethroid resistance in the major malaria vector *Anopheles funestus*. *Parasites & Vectors* **2010**, *3*, 1–7.

[9] Ahmad, M.; Denholm, I.; Bromilow, R. H. Delayed cuticular penetration and enhanced

metabolism of deltamethrin in pyrethroid-resistant strains of *Helicoverpa armigera* from China and Pakistan. *Pest Management Science* **2006**, *62*, 805–810.

[10] Balabanidou, V.; Grigoraki, L.; Vontas, J. Insect cuticle: a critical determinant of insecticide resistance. *Current Opinion in Insect Science* **2018**, *27*, 68–74.

[11] Cava, D.; Catala, R.; Gavara, R.; Lagaron, J. M. Testing limonene diffusion through food contact polyethylene by FT-IR spectroscopy: film thickness, permeant concentration and outer medium effects. *Polymer Testing* **2005**, *24*, 483–489.

[12] McAuley, W.; Lad, M.; Mader, K.; Santos, P.; Tetteh, J.; Kazarian, S.; Hadgraft, J.; Lane, M. ATR-FTIR spectroscopy and spectroscopic imaging of solvent and permeant diffusion across model membranes. *European Journal of Pharmaceutics and Biopharmaceutics* **2010**, *74*, 413–419.

[13] Fieldson, G.; Barbari, T. The use of FTIR-ATR spectroscopy to characterize penetrant diffusion in polymers. *Polymer* **1993**, *34*, 1146–1153.

[14] Di Cagno, M. P.; Clarelli, F.; VaŁbenø, J.; Lesley, C.; Rahman, S. D.; Cauzzo, J.; Franceschinis, E.; Realdon, N.; Stein, P. C. Experimental determination of drug diffusion coefficients in unstirred aqueous environments by temporally resolved concentration measurements. *Molecular Pharmaceutics* **2018**, *15*, 1488–1494.

[15] Kunz, M.; Staiger, S.; Burghardt, M.; Popp, C.; George, N.; Roberts, K.; Riederer, M. Diffusion Kinetics of Active Ingredients and Adjuvants in Wax Films: An Attenuated Total Reflection-Infrared Spectroscopy Study of a Leaf Surface Model. *ACS Agricultural Science & Technology* **2022**, *2*, 625–638.

[16] Mirabella Jr, F. M. Surface orientation of polypropylene. II. Determination for uniaxially and biaxially oriented films using internal reflection spectroscopy. *Journal of Polymer Science: Polymer Physics Edition* **1984**, *22*, 1293–1304.

[17] Yuan, P.; Sung, C. S. P. Angular characterization of polymer surfaces by FTIR ATR dichroism with a rotatable truncated hemispheric crystal. *Macromolecules* **1991**, *24*, 6095–6103.

[18] Vorenkamp, E.; Van Ruiten, J.; Kroesen, F.; Meyer, J.; Hoekstra, J.; Challa, G. Interdiffusion and adhesion of poly(vinyl-chloride) and poly(methyl methacrylate). *Polymer Communications* **1989**, *30*, 116–120.

[19] High, M. S.; Painter, P. C.; Coleman, M. M. Polymer-polymer mutual diffusion using transmission FTIR spectroscopy. *Macromolecules* **1992**, *25*, 797–801.

[20] Breitmaier, E. *Terpenes: flavors, fragrances, pharmaca, pheromones*; John Wiley & Sons, 2006.

[21] Tanzi, C. D.; Vian, M. A.; Ginies, C.; Elmaataoui, M.; Chemat, F. Terpenes as green solvents for extraction of oil from microalgae. *Molecules* **2012**, *17*, 8196–8205.

[22] Morcia, C.; Tumino, G.; Ghizzoni, R.; Terzi, V. Carvone (*Mentha spicata L.*) oils. *Essential Oils in Food Preservation, Flavor and Safety* **2016**, 309–316.

[23] EPA: Biopesticides Registration Action Document: l-Carvone. 2009.

[24] De Carvalho, C. C.; Da Fonseca, M. M. R. Carvone: Why and how should one bother to produce this terpene? *Food Chemistry* **2006**, *95*, 413–422.

[25] Vogt, T. Phenylpropanoid biosynthesis. *Molecular Plant* **2010**, *3*, 2–20.

[26] Cheng, S.-S.; Liu, J.-Y.; Tsai, K.-H.; Chen, W.-J.; Chang, S.-T. Chemical composition and mosquito larvicidal activity of essential oils from leaves of different Cinnamomum osmophloeum provenances. *Journal of Agricultural and Food Chemistry* **2004**, *52*, 4395–4400.

[27] Chang, K.-S.; Tak, J.-H.; Kim, S.-I.; Lee, W.-J.; Ahn, Y.-J. Repellency of cinnamomum cassia bark compounds and cream containing cassia oil to Aedes aegypti (Diptera: Culicidae) under laboratory and indoor conditions. *Pest Management Science: formerly Pesticide Science* **2006**, *62*, 1032–1038.

[28] Carnauba wax, Thermo Scientific Chemicals. https://www.fishersci.at/shop/products/carnauba-wax-thermo-scientific/11327408, Accessed: 2024-06-15.

[29] Vandenburg, L.; Wilder, E. The structural constituents of carnauba wax. *Journal of the American Oil Chemists Society* **1970**, *47*, 514–518.

[30] Palou, A.; Cruz, J.; Blanco, M.; Larraz, R.; Frontela, J.; Bengoechea, C. M.; Gonzalez, J. M.; Alcala, M. Characterization of the composition of paraffin waxes on industrial applications. *Energy & Fuels* **2014**, *28*, 956–963.

[31] Seyer, W.; Inouye, K. Paraffin wax tensile strength and density at various temperatures. *Industrial & Engineering Chemistry* **1935**, *27*, 567–570.

[32] Bogdanov, S. Beeswax: History, uses and trade. *Bee Product Science* **2016**, *25*, 1–18.

[33] Bernal, J. L.; Jiménez, J. J.; del Nozal, M. J.; Toribio, L.; Martín, M. T. Physico-chemical parameters for the characterization of pure beeswax and detection of adulterations. *European Journal of Lipid Science and Technology* **2005**, *107*, 158–166.

[34] Tulloch, A. P. Beeswax: composition and analysis. *Bee world* **1980**, *61*, 47–62.

[35] Tulloch, A.; Hoffman, L. Canadian beeswax: analytical values and composition of hydrocarbons, free acids and long chain esters. *Journal of the American Oil Chemists Society* **1972**, *49*, 696–699.

[36] Harris, C. R. et al. Array programming with NumPy. *Nature* **2020**, *585*, 357362.